

What can we learn from the directed flow in heavy-ion collisions at BES RHIC energies?

Yu. B. Ivanov^{1,2} and A. A. Soldatov²

¹ National Research Centre "Kurchatov Institute" (NRC "Kurchatov Institute"), Moscow 123182, Russia

² National Research Nuclear University "MEPhI" (Moscow Engineering Physics Institute), Moscow 115409, Russia

Received: date / Revised version: date

Abstract. Analysis of directed flow (v_1) of protons, antiprotons and pions in heavy-ion collisions is performed in the range of collision energies $\sqrt{s_{NN}} = 2.7\text{--}39$ GeV. Simulations have been done within a three-fluid model employing a purely hadronic equation of state (EoS) and two versions of the EoS with deconfinement transitions: a first-order phase transition and a smooth crossover transition. The crossover EoS is unambiguously preferable for the description of the most part of experimental data in this energy range. The directed flow indicates that the crossover deconfinement transition takes place in semicentral Au+Au collisions in a wide range of collision energies $4 \lesssim \sqrt{s_{NN}} \lesssim 30$ GeV. The obtained results suggest that the deconfinement EoS's in the quark-gluon sector should be stiffer at high baryon densities than those used in the calculation. The latter finding is in agreement with that discussed in astrophysics.

PACS. 25.75.-q , 25.75.Nq, 24.10.Nz

1 Introduction

The directed flow [1] is one of the key observables in heavy ion collisions. Nowadays it is defined as the first coefficient, v_1 , in the Fourier expansion of a particle distribution, $d^2N/dy d\phi$, in azimuthal angle ϕ with respect to the reaction plane [2, 3]

$$\frac{d^2N}{dy d\phi} = \frac{dN}{dy} \left(1 + \sum_{n=1}^{\infty} 2 v_n(y) \cos(n\phi) \right), \quad (1)$$

where y is the longitudinal rapidity of a particle. The directed flow is mainly formed at an early (compression) stage of the collisions and hence is sensitive to early pressure gradients in the evolving nuclear matter [4, 5]. As the EoS is harder, stronger pressure is developed. Thus the directed flow probes the stiffness of the nuclear EoS at the early stage of nuclear collisions [6], which is of prime interest for heavy-ion research.

In Refs. [7, 8, 9], a significant reduction of the directed flow in the first-order phase transition to the quark-gluon phase (QGP) (the so-called "softest-point" effect) was predicted, which results from decreasing the pressure gradients in the mixed phase as compared to those in pure hadronic and quark-gluon phases. It was further predicted [10, 11, 12] that the directed flow as a function of rapidity exhibits a wiggle near the midrapidity with a negative slope near the midrapidity, when the incident energy is in the range corresponding to onset of the first-order phase transition. Thus, the wiggle near the midrapidity

and the wiggle-like behavior of the excitation function of the midrapidity v_1 slope were put forward as a signature of the QGP phase transition. However, the QGP EoS is not a necessarily prerequisite for occurrence of the midrapidity v_1 wiggle [13]: A certain combination of space-momentum correlations may result in a negative slope in the rapidity dependence of the directed flow in high-energy nucleus-nucleus collisions.

The directed flow of identified hadrons—protons, antiprotons, positive and negative pions—in Au+Au collisions was recently measured in the energy range $\sqrt{s_{NN}} = (7.7\text{--}39)$ GeV by the STAR collaboration within the framework of the beam energy scan (BES) program at the BNL Relativistic Heavy Ion Collider (RHIC) [14]. These data have been already discussed in Refs. [15, 16, 17]. The Frankfurt group [15] did not succeed to describe the data and to obtain conclusive results. Within a hybrid approach [18], the authors found that there is no sensitivity of the directed flow on the EoS and, in particular, on the occurrence of a first-order phase transition. One of the possible reasons of this result can be that the initial stage of the collision in all scenarios is described within the Ultra-relativistic Quantum Molecular Dynamics (UrQMD) [19] in the hybrid approach. However, this initial stage does not solely determine the final directed flow because the UrQMD results still differ from those obtained within the hybrid approach [18].

In Refs. [16, 17] the new STAR data were analyzed within two complementary approaches: kinetic transport approaches of the parton-hadron string dynamics (PHSD)

[20] and its purely hadronic version (HSD) [21]), and a hydrodynamic approach of the relativistic three-fluid dynamics (3FD) [22, 23]. In contrast to other observables, the directed flow was found to be very sensitive to the accuracy settings of the numerical scheme. Accurate calculations require a very high memory and computation time. Due to this reason in Refs. [16, 17] we failed to perform calculations for energies above $\sqrt{s_{NN}} = 30$ GeV within the 3FD model.

In the present paper we extend the analysis performed in Refs. [16, 17] within the 3FD model. We succeeded to perform simulations at $\sqrt{s_{NN}} = 39$ GeV, which allow us to strengthen conclusions on the relevance of used EoS's, in particular, on the stiffness of the EoS at high baryon densities in the QGP sector and outline the range of the crossover transition to the QGP in terms of collision energy.

2 The 3FD model

The 3FD approximation is a minimal way to simulate the early-stage nonequilibrium state of the colliding nuclei at high incident energies. The 3FD model [22] describes a nuclear collision from the stage of the incident cold nuclei approaching each other, to the final freeze-out stage. Contrary to the conventional one-fluid dynamics, where a local instantaneous stopping of matter of the colliding nuclei is assumed, the 3FD considers inter-penetrating counter-streaming flows of leading baryon-rich matter, which gradually decelerate each other due to mutual friction. The basic idea of a 3FD approximation to heavy-ion collisions is that a generally nonequilibrium distribution of baryon-rich matter at each space-time point can be represented as a sum of two distinct contributions initially associated with constituent nucleons of the projectile and target nuclei. In addition, newly produced particles, populating predominantly the midrapidity region, are attributed to a third, so-called fireball fluid that is governed by the net-baryon-free sector of the EoS.

At the final stage of the collision the p- and t-fluids are either spatially separated or mutually stopped and unified, while the f-fluid, predominantly located in the midrapidity region, keeps its identity and still overlaps with the baryon-rich fluids to a lesser (at high energies) or greater (at lower energies) extent. In particular, the friction between the baryon-rich and net-baryon-free fluids is the only source of dissipation at this final stage because each separate fluid is described by equations of the ideal hydrodynamics with the right-hand sides containing friction with other fluids. All the observables in the 3FD model are composed of contributions from all three fluids. Of course, relative fractions of these contributions depend on multiple factors, in particular, on the rapidity range. The freeze-out is performed accordingly to the procedure described in Ref. [22] and in more detail in Refs. [24, 25]. This is a so-called modified Milekhin scheme that conserves the energy, momentum and baryon number. The freeze-out criterion is based on a local energy density, ε_{tot} , defined as a sum of contributions from all (p-, t- and f-) fluids being

present in a local space-time region. The freeze-out procedure starts if $\varepsilon_{tot} < \varepsilon_{frz}$. The freeze-out energy density $\varepsilon_{frz} = 0.4$ GeV/fm³ was chosen mostly on the condition of the best reproduction of secondary particle yields.

Different EoS's can be implemented in the 3FD model. A key point is that the 3FD model is able to treat a deconfinement transition at the early *nonequilibrium* stage of the collision, when the directed flow is mainly formed. In this work we apply a purely hadronic EoS [26], an EoS with a crossover transition as constructed in Ref. [27] and an EoS with a first-order phase transition into the QGP [27]. These are illustrated in Fig. 1. Note that an onset of deconfinement in the 2-phase EoS takes place at rather high baryon densities, above $n \sim 8 n_0$. In EoS's compatible with constraints on the occurrence of the quark matter phase in massive neutron stars, the phase coexistence starts at about $4 n_0$ [28]. As it will be seen below, this excessive softness of the deconfinement EoS's of Ref. [27] is an obstacle for proper reproduction of the directed flow at high collision energies.

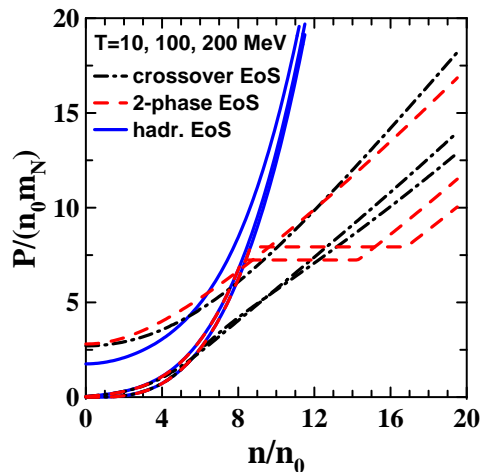


Fig. 1. Pressure scaled by the product of normal nuclear density ($n_0 = 0.15$ fm⁻³) and nucleon mass (m_N) versus baryon density (scaled by n_0) for three considered EoS's. Results are presented for three different temperatures $T = 10, 100$ and 200 MeV (bottom-up for corresponding curves).

In recent papers [23, 29, 30, 31, 32, 33, 34] a large variety of bulk observables has been analyzed with these three EoS's: the baryon stopping [23, 31], yields of different hadrons, their rapidity and transverse momentum distributions [29, 30, 32], the elliptic flow of various species [33, 34]. This analysis has been done in the same range of incident energies as that in the present paper. Comparison with available data indicated a definite advantage of the deconfinement scenarios over the purely hadronic one especially at high collision energies. As an example, excitation functions of average transverse masses ($\langle m_T \rangle - m$) of protons, antiprotons and pions are presented in Fig. 2. This quantity characterizes the transverse radial flow in the reaction and hence is relevant to the directed flow discussed here. In Fig. 2 the 3FD results on $\langle m_T \rangle$ are confronted

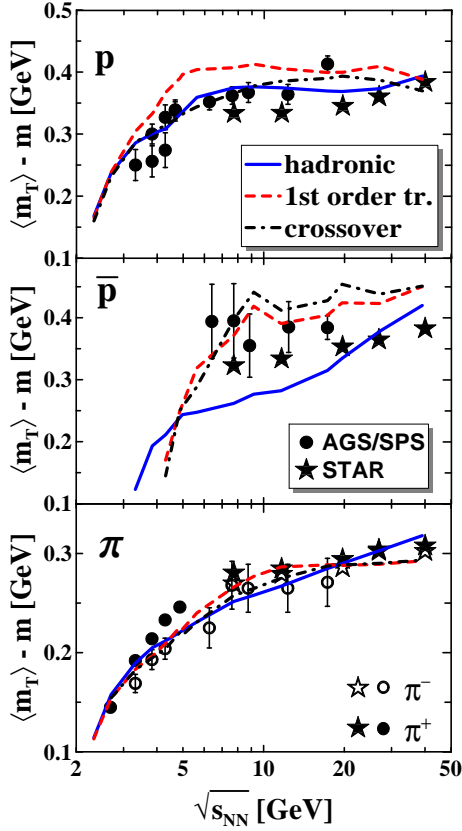


Fig. 2. Average transverse mass (minus particle mass) at midrapidity of protons (p), antiprotons (\bar{p}) and pions (π) from central ($b = 2$ fm) Au+Au collisions as functions of the collision energy. Experimental data are taken from Refs. [35,36,37,38,39] for AGS, [40,41,42,43] for SPS and [44] for BES-RHIC energies.

to old AGS/SPS data [35,36,37,38,39,40,41,42,43] and also compared with new data from the STAR collaboration [44]. On the average, the crossover scenario still looks preferable, though these new STAR data are somewhat below those from SPS (for protons and antiprotons). It could seem that the crossover and hadronic scenarios reproduce (or fail to reproduce) the antiproton STAR data to the same extent. However, the slope of the crossover curve is definitely more adequate to the data. The first-order-transition scenario certainly fails for protons in the energy region where onset of deconfinement takes place in this EoS. The observed step-like behavior of the $\langle m_T \rangle$ excitation functions originates from peculiarities of the freeze-out in the 3FD model, as it is discussed in Ref. [30] in detail. The physical pattern behind this freeze-out resembles the process of expansion of compressed and heated classical fluid into vacuum, mechanisms of which were studied both experimentally and theoretically. The freeze-out is associated with evaporation from the surface of the expanding fluid and sometimes with the explosive transformation of the strongly superheated fluid to the gas.

The physical input of the present 3FD calculations is described in detail in Ref. [23].

3 Results

The 3FD simulations were performed for mid-central Au+Au collisions, i.e. at impact parameter $b = 6$ fm. In Ref. [45] the values of the impact parameter corresponding to the experimental range of 10–40% most central collisions were obtained using a Monte-Carlo Glauber calculation. The range of $b \approx 4.7$ –9.4 fm was found. This range manifested very weak collision-energy dependence. The mean value of this range is $\langle b \rangle \approx 7$ fm, which is usually used for representative calculations for this centrality bin, see e.g. PHSD/HSD calculations in Ref. [16]. The Glauber calculation [45] was based on a Woods-Saxon density profile with the diffuseness parameter ≈ 0.5 fm and resulted in the total hadronic cross-section for Au+Au collisions $\sigma_{AA} \simeq 720$ barns. Within the 3FD model the initial nuclei are represented by sharp-edged spheres, i.e. with zero diffuseness. This is done for stability of the incident nuclei before collision [22]. Under this approximation the total hadronic Au+Au cross-section turns out to be $\sigma_{AA}^{3FD} \simeq 580$ barns. Therefore, we have to accordingly scale the mean value of the impact parameter as $\langle b^{3FD} \rangle \approx \langle b \rangle (\sigma_{AA}^{3FD} / \sigma_{AA})^{1/2} \approx 6$ fm. This justifies our choice of the representative b . Following the experimental conditions, the acceptance $p_T < 2$ GeV/c for transverse momentum (p_T) of the produced particles is applied to all considered hadrons. The directed flow $v_1(y)$ as a function of rapidity y at BES-RHIC bombarding energies is presented in Fig. 3 for pions, protons and antiprotons.

As seen, the first-order-transition scenario gives results for the proton v_1 which strongly differ from those in the crossover scenario at $\sqrt{s_{NN}} = 7.7$ and 19.6 GeV. This is in contrast to other bulk observables analyzed so far [23,29,30,31,32,33,34]. At $\sqrt{s_{NN}} = 39$ GeV the directed flow of all considered species practically coincidence within the first-order-transition and crossover scenarios. It means that the crossover transition to the QGP has been practically completed at $\sqrt{s_{NN}} = 39$ GeV. It also suggests that the region $7.7 \leq \sqrt{s_{NN}} \leq 30$ GeV, where the crossover EoS provides the best (although not perfect) overall reproduction of the STAR data, is the region of the crossover transition.

The crossover EoS is definitely the best in reproduction of the proton $v_1(y)$ at $\sqrt{s_{NN}} \leq 20$ GeV. However, surprisingly the hadronic scenario becomes preferable for the proton $v_1(y)$ at $\sqrt{s_{NN}} > 20$ GeV. A similar situation takes place in the PHSD/HSD transport approach. Indeed, predictions of the HSD model (i.e. without the deconfinement transition) for the proton $v_1(y)$ become preferable at $\sqrt{s_{NN}} > 30$ GeV [16], i.e. at somewhat higher energies than in the 3FD model. Moreover, the proton v_1 predicted by the UrQMD model, as cited in the experimental paper [14] and in the recent theoretical work [15], better reproduces the proton $v_1(y)$ data at high collision energies than the PHSD and 3FD-deconfinement models do. Note that the UrQMD model is based on the hadronic dynamics. All these observations could be considered as an evidence of a problem in the QGP sector of a EoS. At the same time the antiproton directed flow at $\sqrt{s_{NN}} > 10$ GeV definitely in-

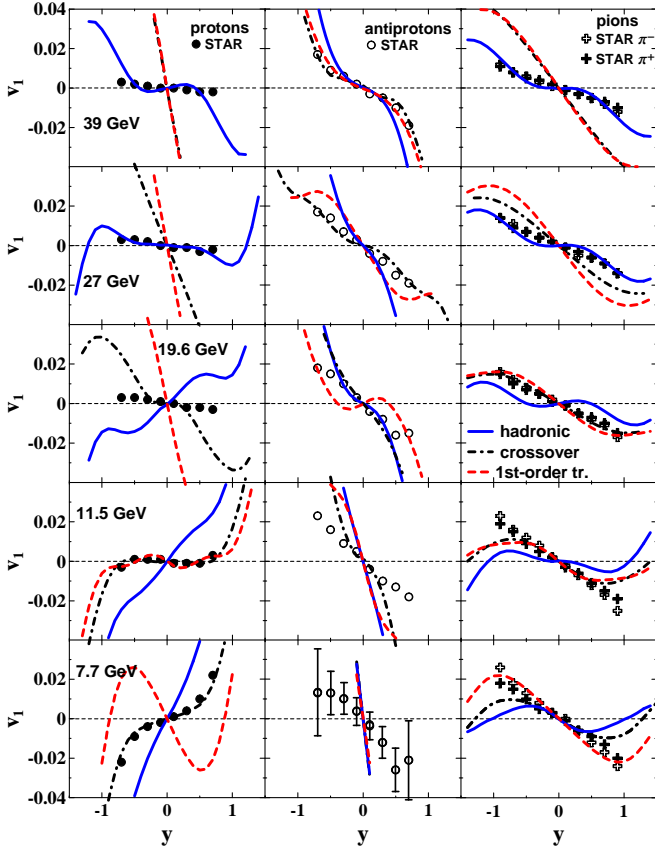


Fig. 3. The directed flow $v_1(y)$ for protons, antiprotons and pions from mid-central ($b = 6$ fm) Au+Au collisions at $\sqrt{s_{NN}} = 7.7$ –39 GeV calculated with different EoS's. Experimental data are from the STAR collaboration [14].

indicates a preference of the crossover scenario within both the PHSD/HSD and 3FD approaches.

This puzzle has a natural resolution within the 3FD model. The the QGP sector of the EoS's with deconfinement [27] was fitted to the lattice QCD data at zero net-baryon density and just extrapolated to nonzero baryon densities. The protons mainly originate from baryon-rich fluids that are governed by the EoS at finite baryon densities. The too strong proton antiflow within the crossover scenario at $\sqrt{s_{NN}} > 20$ GeV is a sign of too soft QGP EoS at high baryon densities. In general, the antiflow or a weak flow indicates softness of an EoS [6, 7, 8, 9, 10, 11, 12, 13]. Predictions of the first-order-transition EoS, the QGP sector of which is constructed in the same way as that of the crossover one, fail even at lower collision energies, when the QGP starts to dominate in the collision dynamics, i.e. at $\sqrt{s_{NN}} \gtrsim 15$ GeV. This fact also supports the conjecture on a too soft QGP sector at high baryon densities in the used EoS's.

At the same time, the net-baryon-free (fireball) fluid is governed by the EoS at zero net-baryon density. This fluid is a main source of antiprotons (more than 80% near midrapidity at $\sqrt{s_{NN}} > 20$ GeV and $b = 6$ fm), $v_1(y)$ of which is in good agreement with the data at $\sqrt{s_{NN}} > 20$ GeV within the crossover scenario and even in perfect

agreement – within the first-order-transition scenario at $\sqrt{s_{NN}} = 39$ GeV. It is encouraging because at zero net-baryon density the QGP sector of the EoS's is fitted to the lattice QCD data and therefore can be trusted. The crossover scenario, as well as all other scenarios, definitely fails to reproduce the antiproton $v_1(y)$ data at 7.7 GeV. The reason is low multiplicity of produced antiprotons. The antiproton multiplicity in the mid-central ($b = 6$ fm) Au+Au collision at 7.7 GeV is 1 within the deconfinement scenarios and 3 within the hadronic scenario. Therefore, the hydrodynamical approach based on the grand canonical ensemble is certainly inapplicable to the antiprotons in this case. The grand canonical ensemble, with respect to conservation laws, gives a satisfactory description of abundant particle production in heavy ion collisions. However, when applying the statistical treatment to rare probes one needs to treat the conservation laws exactly, that is the canonical approach. The exact conservation of quantum numbers is known to reduce the phase space available for particle production due to additional constraints appearing through requirements of local quantum number conservation. An example of applying the canonical approach to the strangeness production can be found in [46] and references therein.

The pions are produced from all fluids: near midrapidity $\sim 60\%$ from the baryon-rich fluids and $\sim 40\%$ from the net-baryon-free one at $\sqrt{s_{NN}} > 20$ GeV. Hence, the disagreement of the pion v_1 with data, resulting from redundant softness of the QGP EoS at high baryon densities, is moderate at $\sqrt{s_{NN}} > 20$ GeV. In general, the pion v_1 is less sensitive to the EoS as compared to the proton and antiproton ones. As seen from Fig. 3, the deconfinement scenarios are definitely preferable for the pion $v_1(y)$ at $\sqrt{s_{NN}} < 20$ GeV. Though, the hadronic-scenario results are not too far from the experimental data. At $\sqrt{s_{NN}} = 39$ GeV the hadronic scenario gives even the best description of the pion data because of a higher stiffness of the hadronic EoS at high baryon densities, as compared with that in the considered versions of the QGP EoS.

Thus, all the analyzed data testify in favor of a harder QGP EoS at high baryon densities than those used in the simulations, i.e. the desired QGP EoS should be closer to the used hadronic EoS at the same baryon densities (see Fig. 1). At the same time, a moderate softening of the QGP EoS at moderately high baryon densities is in agreement with data at $7.7 \lesssim \sqrt{s_{NN}} \lesssim 20$ GeV.

Here it is appropriate to mention a discussion on the QGP EoS in astrophysics. In Ref. [47] it was demonstrated that the QGP EoS can be almost indistinguishable from the hadronic EoS at high baryon densities relevant to neutron stars. In particular, this gives a possibility to explain hybrid stars with masses up to about 2 solar masses (M_\odot), in such a way that “hybrid stars masquerade as neutron stars” [47]. The discussion of such a possibility has been revived after measurements on two binary pulsars PSR J1614-2230 [48] and PSR J0348+0432 [49] resulted in the pulsar masses of $(1.97 \pm 0.04)M_\odot$ and $(2.01 \pm 0.04)M_\odot$, respectively. The obtained results on the directed flow give

us another indication of a required hardening of the QGP EoS at high baryon densities.

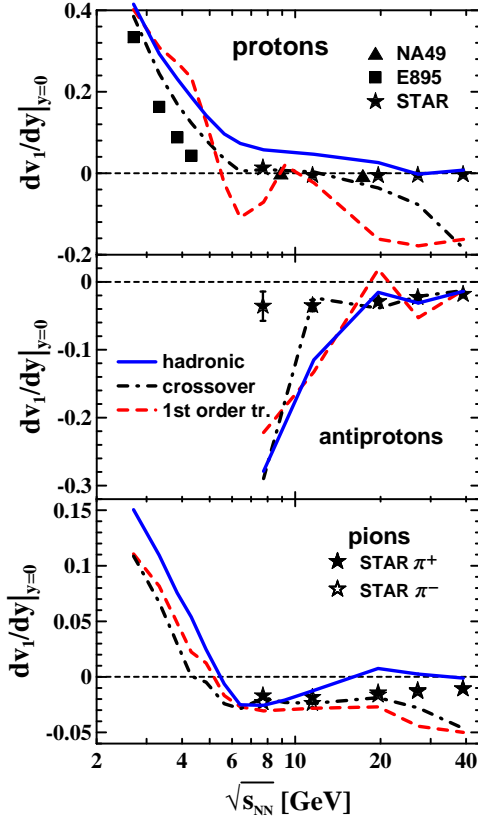


Fig. 4. The beam energy dependence of the directed flow slope at midrapidity for protons, antiprotons and pions from mid-central ($b = 6$ fm) Au+Au collisions calculated with different EoS's. The experimental data are from Refs. [14, 51, 50].

The slope of the directed flow at the midrapidity is often used to quantify variation of the directed flow with collision energy. The excitation functions for the slopes of the v_1 distributions at midrapidity are summarized in Fig. 4, where earlier experimental results from the AGS [50] and SPS [51] are also presented. As noted above, the best reproduction of the data is achieved with the crossover EoS. The proton dv_1/dy within the first-order-transition scenario exhibits a wiggle earlier predicted in Refs. [8, 9, 11, 12]. The first-order-transition results demonstrate the worst agreement with the proton and antiproton data on dv_1/dy . The discrepancies between experiment and the 3FD predictions are smaller for the purely hadronic EoS, however, the agreement for the crossover EoS is definitely better though it is far from being perfect. As seen from Fig. 4, the rising transparency of colliding nuclei makes the proton v_1 slope to be close to zero even for comparatively hard hadronic EoS.

The above discussed problems of the crossover scenario reveal themselves also in the dv_1/dy plot. At high energies ($\sqrt{s_{NN}} > 20$ GeV), the slopes also indicate that the used deconfinement EoS's in the quark-gluon sector at zero baryon chemical potential are quite suitable for

reproduction of the antiproton dv_1/dy while those at high baryon densities (proton slope) should be stiffer in order to achieve better description of proton dv_1/dy . A combined effect of this excessive softness of the QGP EoS and the reducing baryon stopping results in more and more negative proton slopes at high collision energies. This is in line with the mechanism discussed in Ref. [13]. The pion flow partially follows the proton pattern, as discussed above. Therefore, the pion v_1 slope also becomes more negative with energy rise. As for the poor reproduction of the proton v_1 slope at low energies ($\sqrt{s_{NN}} < 5$ GeV), it is still questionable because the same data but in terms of the transverse in-plane momentum, $\langle P_x \rangle$, are almost perfectly reproduced by the crossover scenario [17]. It is difficult to indicate the beginning of the crossover transition because the crossover results become preferable beginning with relatively low collision energies ($\sqrt{s_{NN}} > 3$ GeV). However, the beginning of the crossover transition can be approximately pointed out as $\sqrt{s_{NN}} \simeq 4$ GeV.

Of course, the 3FD model does not include all factors determining the directed flow. Initial-state fluctuations, which in particular make the directed flow to be nonzero even at midrapidity, are out of the scope of the 3FD approach. Apparently, these fluctuations can essentially affect the directed flow at high collision energies, when the experimental flow itself is very weak. Another point is so-called afterburner, i.e. the kinetic evolution after the hydrodynamical freeze-out. This stage is absent in the conventional version of the 3FD. Recently Iu. Karpenko constructed an event generator based on the output of the 3FD model. Thus constructed particle ensemble can be further evolved within the UrQMD model. Preliminary results [52] show that such kind of the afterburner mainly affects the pion v_1 at peripheral rapidities. At $\sqrt{s_{NN}} < 5$ GeV, the midrapidity region of the pion v_1 is also affected.

4 Conclusions

In conclusion, the crossover EoS is unambiguously preferable for the the most part of experimental data in the considered energy range, though this description is not perfect. Based on the crossover EoS of Ref. [27], the directed flow in semicentral Au+Au collisions indicates that the crossover deconfinement transition takes place in the wide range incident energies $4 \lesssim \sqrt{s_{NN}} \lesssim 30$ GeV. In part, this wide range could be a consequence of that the crossover transition constructed in Ref. [27] is very smooth. In this respect, this version of the crossover EoS certainly contradicts results of the lattice QCD calculations, where a fast crossover, at least at zero chemical potential, was found [53].

At highest computed energies of $\sqrt{s_{NN}} > 20$ GeV, the obtained results indicate that the deconfinement EoS's in the QGP sector should be stiffer at high baryon densities than those used in the calculation, i.e. more similar to the purely hadronic EoS. This observation is in agreement with that discussed in astrophysics.

In view of this similarity of the QGP and hadronic EoS's at high baryon densities a question arises if we can

use the directed flow to detect the deconfinement transition. Qualitatively, a wiggle in the excitation function of the net-proton v_1 slope could be a signal of the QGP formation. This signal is unavoidable because of the EoS softening in the transition range from hadronic phase to the QGP. In fact, such a weak wiggle is observed in the STAR data [14]. However, this signal is still ambiguous because the corresponding antiproton flow can be of pure hadronic nature, as it was pointed out in Ref. [13]. Therefore, we are left with a routine way of comparing predictions of various EoS's (with and without deconfinement) with the v_1 experimental data. This will hopefully give us a reliable evidence on the QGP formation.

Fruitful discussions with D. Blaschke, W. Cassing, V. P. Konchakovski, V. D. Toneev, and D.N. Voskresensky are gratefully acknowledged. We are grateful to A.S. Khvorostukhin, V.V. Skokov, and V.D. Toneev for providing us with the tabulated first-order-phase-transition and crossover EoS's. The calculations were performed at the computer cluster of GSI (Darmstadt). This work was partially supported by grant NS-932.2014.2.

References

1. P. Danielewicz and G. Odyniec, Phys. Lett. B **157**, 146 (1985).
2. S. Voloshin and Y. Zhang, Z. Phys. C **70**, 665 (1996).
3. S. A. Voloshin, A. M. Poskanzer and R. Snellings, in *Relativistic Heavy Ion Physics*, Landolt-Boernstein New Series, I/23, edited by R. Stock (Springer-Verlag, New York, 2010).
4. H. Sorge, Phys. Rev. Lett. **78**, 2309 (1997).
5. N. Herrmann, J. P. Wessels, and T. Wienold, Ann. Rev. Nucl. Part. Sci. **49**, 581 (1999).
6. V. N. Russkikh, and Yu. B. Ivanov, Phys. Rev. C **74**, 034904 (2006).
7. C. M. Hung and E. V. Shuryak, Phys. Rev. Lett. **75**, 4003 (1995).
8. D. H. Rischke, Y. Pursun, J. A. Maruhn, H. Stöcker, and W. Greiner, Heavy Ion Phys. **1**, 309 (1995).
9. D. H. Rischke, Nucl. Phys. A **610**, 88 (1996).
10. L. P. Csernai and D. Rohrich, Phys. Lett. B **458**, 454 (1999).
11. J. Brachmann *et al.* Phys. Rev. C **61**, 024909 (2000).
12. H. Stöcker, Nucl. Phys. A **750**, 121 (2005).
13. R. J. M. Snellings, H. Sorge, S. A. Voloshin, F. Q. Wang, and N. Xu, Phys. Rev. Lett. **84**, 2803 (2000).
14. L. Adamczyk *et al.* [STAR Collaboration], Phys. Rev. Lett. **112**, 162301 (2014).
15. J. Steinheimer, J. Auvinen, H. Petersen, M. Bleicher and H. Stöcker, Phys. Rev. C **89**, 054913 (2014).
16. V. P. Konchakovski, W. Cassing, Yu. B. Ivanov and V. D. Toneev, Phys. Rev. C **90**, 014903 (2014).
17. Y. B. Ivanov and A. A. Soldatov, Phys. Rev. C **91**, 024915 (2015).
18. H. Petersen, J. Steinheimer, G. Bureau, M. Bleicher and H. Stöcker, Phys. Rev. C **78**, 044901 (2008).
19. S. Bass, *et al.*, Prog. Part. Nucl. Phys. **41**, 225 (1998).
20. W. Cassing, E. L. Bratkovskaya, Nucl. Phys. A **831**, 215 (2009).
21. W. Cassing and E. L. Bratkovskaya, Phys. Rep. **308**, 65 (1999).
22. Yu. B. Ivanov, V. N. Russkikh, and V. D. Toneev, Phys. Rev. C **73**, 044904 (2006).
23. Yu. B. Ivanov, Phys. Rev. C **87**, 064904 (2013).
24. V. N. Russkikh and Yu. B. Ivanov, Phys. Rev. C **76**, 054907 (2007).
25. Yu. B. Ivanov and V. N. Russkikh, Phys. Atom. Nucl. **72**, 1238 (2009).
26. V. M. Galitsky and I. N. Mishustin, Sov. J. Nucl. Phys. **29**, 181 (1979).
27. A. S. Khvorostukhin, V. V. Skokov, K. Redlich, and V. D. Toneev, Eur. Phys. J. **C48**, 531 (2006).
28. T. Klähn, R. Lastowiecki and D. B. Blaschke, Phys. Rev. D **88**, no. 8, 085001 (2013).
29. Yu. B. Ivanov, Phys. Rev. C **87**, 064905 (2013).
30. Yu. B. Ivanov, Phys. Rev. C **89**, 024903 (2014).
31. Yu. B. Ivanov, Phys. Lett. B **721**, 123 (2013).
32. Yu. B. Ivanov, Phys. Lett. B **726**, 422 (2013).
33. Yu. B. Ivanov, Phys. Lett. B **723**, 475 (2013).
34. Y. B. Ivanov and A. A. Soldatov, Phys. Rev. C **91**, 024914 (2015).
35. L. Ahle *et al.* [E866 and E917 Collaborations], Phys. Lett. B **476**, 1 (2000).
36. J. L. Klay *et al.* [E895 Collaboration], Phys. Rev. Lett. **88**, 102301 (2002).
37. J. Barrette *et al.* [E877 Collaboration], Phys. Rev. C **62**, 024901 (2000).
38. L. Ahle *et al.* [E802 Collaboration], Phys. Rev. C **60**, 064901 (1999).
39. L. Ahle *et al.* [E802 Collaboration], Phys. Rev. C **57**, 466 (1998).
40. S. V. Afanasiev *et al.* [NA49 Collaboration], Phys. Rev. C **66**, 054902 (2002).
41. C. Alt *et al.* [NA49 Collaboration], Phys. Rev. C **77**, 024903 (2008).
42. C. Alt *et al.* [NA49 Collaboration], Phys. Rev. C **73**, 044910 (2006).
43. T. Anticic *et al.* [NA49 Collaboration], Phys. Rev. C **69**, 024902 (2004).
44. L. Kumar [STAR Collaboration], Nucl. Phys. A **931**, 1114 (2014).
45. B. I. Abelev *et al.* [STAR Collaboration], Phys. Rev. C **79**, 034909 (2009).
46. S. Hamieh, K. Redlich and A. Tounsi, Phys. Lett. B **486**, 61 (2000).
47. M. Alford, Astrophys. J. **629**, 969 (2005).
48. P. Demorest, *et al.*, Nature **467**, 1081 (2010).
49. J. Antoniadis, *et al.*, Science **340**, 6131 (2013).
50. H. Liu *et al.* (E895 Collaboration), Phys. Rev. Lett. **84**, 5488 (2000).
51. C. Alt *et al.* (NA49 Collaboration), Phys. Rev. C **68**, 034903 (2003).
52. Iu. Karpenko, P. Batyuk, D. Blaschke, M. Bleicher, H. Petersen, Yu. B. Ivanov, O. Rogachevsky, work in progress.
53. Y. Aoki, G. Endrodi, Z. Fodor, S. D. Katz and K. K. Szabo, Nature **443**, 675 (2006).